Results in Physics 19 (2020) 103653

Contents lists available at ScienceDirect

Results in Physics

journal homepage: www.elsevier.com/locate/rinp

Coupling terahertz wave into a plasmonic waveguide by using two ribbon waveguides

Wenwei Shen [a], Jingya Xie [a], Xiaofei Zang [a], Li Ding [a], Lin Chen [a,b,*]

[a] Shanghai Key Lab of Modern Optical System, University of Shanghai for Science and Technology, Shanghai 200093, China
[b] Shanghai Institute of Intelligent Science and Technology, Tongji University, Shanghai 200092, China

ARTICLE INFO

Keywords:
Waveguides
Surface plasmons
Coupling
Dielectric ribbon waveguide

ABSTRACT

We proposed the design of coupling terahertz wave into a plasmonic waveguide via using two alumina ribbon waveguides. The dispersion relation of fundamental alumina waveguide mode shows that it has intersections with plasmonic modes, resulting in the power transferred efficiently from dielectric waveguide to the structures. In experiment, a dual band metallic waveguide with two different groove depths associated with input and output alumina strips coated by polypropylene is fabricated and measured. Two plasmonic mode bands supported by plasmonic waveguide can be found because the terahertz radiation has been coupled from free space to dielectric ribbon waveguide at resonance frequencies of 0.28 THz and 0.47 THz. This coupling approach opens a novel avenue for coupling terahertz radiation and can be used for developing novel terahertz planar wave devices and circuits.

Introduction

Terahertz (THz) waveguides has recently received widespread attention based on the various application such as sensing, nondestructive testing, security check and high speed communication. There are several designs that can achieve THz waveguides and confinement such as parallel plate waveguides [1–3], plasmonic waveguides [4–8] etc. In the low frequency regime, the structural metal surface can support spoof plasmons [9,10], which can be further used as THz plasmonic waveguides. The plasmonic waveguides have many advantages compared with parallel plate waveguides. For example, the arrays are miniaturized and can be integrated into other functional devices easily. They can also detect small changes of surrounding medium, have highly confinement for THz spoof surface plasmons polaritons (SPPs), and low loss in transmission [11]. Yet, there are several challenges for the coupling of THz wave from free space to plasmonic waveguide due to the mismatch wave vectors between them. In order to explore the propagation property of THz spoof SPPs, it's critical to find a convenient and efficient excitation and detection method.

According to recent research, there are several common excitation methods, such as edge scattering coupling, prism coupling, grating coupling, waveguide coupling and graphene coupling [12–24]. For instance, the edge scattering method is applied to excite larger SPP wave vectors. The broadband THz spoof SPPs can be excited by placing a razor blade above two-dimensional arrays of subwavelength-periodicity pits. The drawbacks of this method are, only small part of wave vector can match the vector of spoof SPPs [12] and the additional blade limits the integration of devices [5]. Prism coupling is also an effective method to excite spoof SPPs with large wave vector. The gap between the base of the prism and the textured metal surface made of periodic grooves influence the coupling effect sensitively [13,14]. The method has strict requirements on the incidence angle and frequency range. However, it is hard to be integrated due to bulk prism. Grating coupling method which is also widely used in the optical range, can transfer to THz frequency [15–17]. The grating consisting of metal sites is designed to match the incident THz wave. The width of metal pillars is also next to the grating so as to guide the excited spoof SPPs to the waveguide. But the fabrication is complex, which impede the real application. The waveguide coupling method can be realized through coupling the THz wave into the flat metal sheet that can support SPPs by using field-confined parallel plate waveguides [18,19]. We note that the SPPs mode shows weak confinement and limits its applications [25]. Therefore, it still needs to find an efficient and convenient method to couple THz waves into the plasmonic waveguide that can support spoof SPPs.

In this study, a new attempt was made to introduce a highly refractive alumina ribbon waveguide as a bridge to achieve effective coupling

* Corresponding author at: Shanghai Key Lab of Modern Optical System, University of Shanghai for Science and Technology, Shanghai 200093, China.
E-mail address: linchen@usst.edu.cn (L. Chen).

https://doi.org/10.1016/j.rinp.2020.103653
Received 12 October 2020; Received in revised form 19 November 2020; Accepted 24 November 2020
Available online 30 November 2020

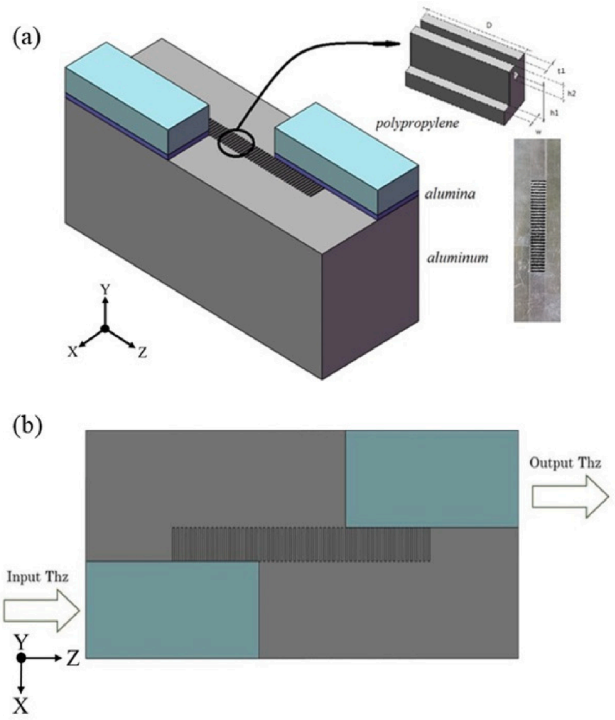

Fig. 1. (a) Three whole view of the planar THz waveguide, two pieces of our so-called ribbon was placed alongside the surface of the metal film to couple the THz radiation into and out of the device. One period of our corrugated metal film, of which the dimensions are: $h_1 = 350$ μm, $h_2 = 150$ μm, $w = 60$ μm, $t_1 = 65$ μm, $D = 700$ μm, $p = 250$ μm, respectively. (The inset is a top view image). (b) The xz-plane view of the planar THz waveguide, two pieces of our so-called ribbon was placed alongside the surface of the metal film to couple the THz radiation into and out of the device.

from free space to the plasmonic waveguide, which, to our knowledge, was not reported before [26]. A thin layer of low loss low-refractive polypropylene is coated upon the alumina ribbon to enhance the localized field and achieve the mode field matching [27–30]. Two pieces of alumina waveguide are placed next to the surface of the metal film as a dielectric coupling waveguide. The main TM_0 mode is activated to ensure that only single mode propagates along the waveguide by controlling the thickness of the alumina [19]. The merits of this proposed structure is the efficient control of THz wave at the circuit level. When the incident wave is coupled to the alumina ribbon waveguide from the input surface of the waveguide, it propagates along the waveguide and transmits energy to the nearby plasmonic waveguide through near-field coupling. Another alumina ribbon waveguide is placed on the opposite side of the plasma waveguide to couple and output THz waves from the plasmonic waveguide. A periodic perforated metal film with composite periodic grooves was fabricated and used as a plasmonic waveguide, which can support dual-band transmission in one waveguide. We investigate the dispersion relation and experimentally observe the transmission properties of the proposed device. From the result we can observed experimentally in the transmissivity spectra with the coupling efficiency is 33% at 0.28 THz and 30% at 0.47 THz normalized by that of ribbon waveguide. Their mode fields are also studied. It is expected to have important application value in microscopic THz transmission and integrated circuit.

Coupling design and discussion

The schematic diagram of the dielectric ribbon along with the double-periodic corrugated metal is showed in Fig. 1(a). Two pieces of alumina ($\varepsilon_r \approx 9.6$) as well as the cladding material which is made of

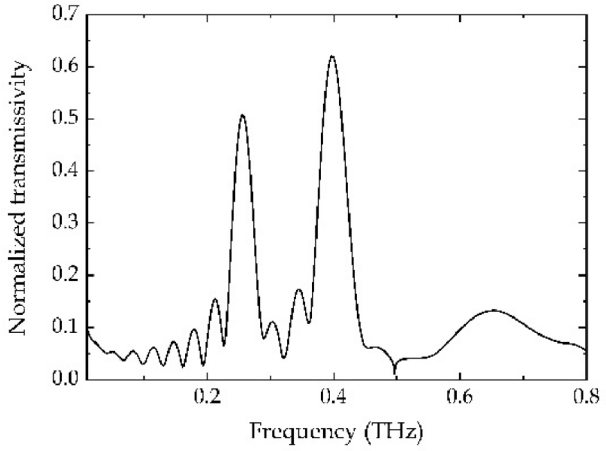

Fig. 2. Simulated transmission spectrum at the output dielectric waveguide port which is normalized by that of ribbon waveguide.

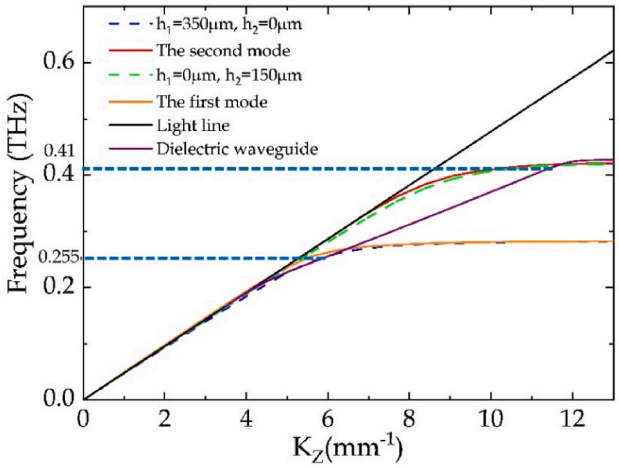

Fig. 3. The dispersion relations of our proposed structure. The orange line and the red line correspond to the first and second modes of the composite-periodic metallic structure, for which the cutoff frequencies are approximate to 0.28 THz and 0.43 THz, respectively, and the black line is the light line in free space. The green and blue line with solid dots corresponds to the dominant mode of two single-periodic structures with groove depth $h_1 = 350$ μm and $h_2 = 150$ μm, respectively. The purple line is the wave mode through the dielectric ribbon waveguide and crosses at 0.27 THz and 0.42 THz. (For interpretation of the references to colour in this figure legend, the reader is referred to the web version of this article.)

polypropylene ($\varepsilon_r \approx 2.28$) were placed alongside the surface of the metal film and became a dielectric ribbon waveguide. The thickness of the alumina and the polypropylene are approximately 20 μm and 1 mm, respectively, and both of their length and width are 5 mm and 2 mm. The detailed discussion of optimum thicknesses of the alumina and the polypropylene can be found in the Supplementary materials [31]. The whole metallic film is made of aluminum (Al) with 12.5 mm long, 4.7 mm wide and 5 mm thick. The aluminum at THz frequencies behaves almost like perfect conductor compared to visible region [32]. The rectangular apertures were fabricated using conventional laser micromachining techniques.

One unit of our corrugated metal film is displayed in the inset of Fig. 1(a), of which the dimensions are: $h_1 = 350$ μm, $h_2 = 150$ μm, $w = 60$ μm, $t_1 = 65$ μm, $D = 700$ μm, $p = 250$ μm, respectively. We simulated the transmitted THz wave forms in the FDTD simulations. The normalized transmissivity of hybrid structure divided by that of ribbon waveguide is plotted in Fig. 2. The two resonance peaks occur at 0.255 THz

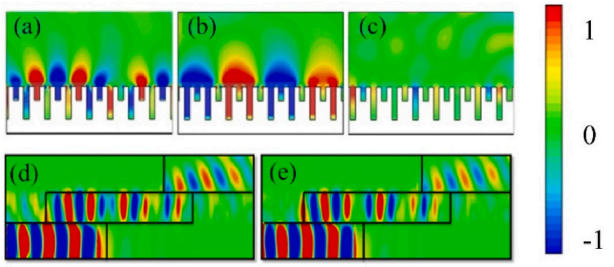

Fig. 4. (a)–(c) The xy-plane view of the normalized electric field calculated at 0.41 THz, 0.255 THz and 0.35 THz respectively. (d), (e) The normalized top view of the electric field at 0.255 THz and 0.41 THz.

and 0.41 THz, respectively.

To obtain the cutoff frequency of dual-band spoof SPPs modes, the dispersion curve of the dual-band grating structure is simulated using the Eigenmode solver in the commercial software CST Microwave Studio, as shown in Fig. 3. The unit cell of single period of plasmonic waveguide is located in an outer air box. A periodic boundary is used in the x direction. The boundaries in the y and z directions are set as perfect electric conductor. The size of the air box is the same as the periodic cell in the x direction and much larger in the y and z directions. The orange line and the red line correspond to the first and second mode of the composite-periodic metallic structure, for which the cutoff frequencies are approximate to 0.28 THz and 0.43 THz, respectively. The black line is the light line in free space. To demonstrate the matching of THz wave vectors in the dielectric ribbon and the plasmonic waveguide, we also simulated the dispersion relation of fundamental TM_0 mode of dielectric ribbon waveguide, which is showed as the purple line. The dielectric waveguide is able to couple a fundamental mode band in the THz spectrum. Its dispersion curve lies to the right of the light line with the increase of the frequency. The line crosses the two plasmonic modes at 0.27 THz and 0.42 THz where the electric field confined tightly around the surface and grooves. When the frequency is slightly less than the intersection, the spoof SPP mode can propagate along the surface and couple into the grating structures. Furthermore, in order to illustrate the independence of the two modes, we adjusted $h_1(h_2)$ to 0 μm, thus turned the structure into single-periodic but with the same period.

The dispersion relations of the dominant modes for the two situations are also shown in Fig. 3, in which the green line with solid dots corresponds to the dominant mode of a single-periodic structure with aperture depth $h = 150$ μm, and the blue line with the solid dots corresponds to $h = 350$ μm. We notice that the cutoff frequencies of these two modes illustrated above are in good match with the original two modes. In other words, the first mode of the double-periodic structure is only determined by the deep grooves and the second mode by the shallow grooves. Since the two THz waves are propagating independently on the metal surface, and dual band spoof surface plasmon polaritons should be achievable [33].

Fig. 4(a)–(c) show the xy-plane view of the electric field. Fig. 4(a) is the electric fields at the resonant frequency of 0.255 THz. At the resonance, the electric fields remain confinement both near the surface and inside the shallow grooves. The same situation goes for the other resonant frequency at 0.41 THz, which the fields are confined in the deep grooves, as displayed in Fig. 4(b). Fig. 4(c) shows the electric fields at 0.35 THz, which lies in the gap between the two bands. We clearly observe that spoof SPPs cannot be supported at this frequency.

In order to display the coupling efficiency more intuitive, Fig. 4(d) and (e) show the top view of the electric field at 0.255 THz and 0.41 THz. The gradual conversion was observed from the excited waveguide mode to the spoof SPPs eigenmode, as shown in the near-field platform. In the beginning of the dielectric waveguide, the input wave propagates with mismatch propagation constants. With the increase of the propagation length, the waveguide field gradually matches the field of spoof SPPs eigenmode. The THz radiation carried by the dielectric waveguide can couple into the metallic waveguide effectively.

The coupling length L_c with respect to the phase difference between spoof SPPs mode and the dielectric waveguide at the same frequency, which is described as

$$\Delta\varphi = (k_{zd} - k_{zm})L_c \tag{1}$$

where k_{zd} is the propagation constants of the dielectric waveguide and k_{zm} is the propagation constants of the spoof SPPs modes. The TM_0 mode of dielectric waveguide propagates a distance, when the phase difference $\Delta\varphi$ reaches π, the maximum power is shifted from dielectric waveguide to the plasmonic waveguide. Then the coupling length can be expressed as [18]

$$L_\pi = \pi/(k_{zd} - k_{km}) \tag{2}$$

The coupling length as a function of frequency is plotted in Fig. 5. We can find that the corresponding coupling length related to the resonant frequency in Fig. 2, which two resonant frequencies are observed at 0.255 THz and 0.41 THz. The propagation constant difference for 0.255 THz and 0.41 THz are 0.803 mm^{-1} and 1.044 mm^{-1}, as marked in the dispersion relation in Fig. 3. Then, by using Eq. (2), L_c is equal to 3.91 mm at 0.255 THz and 3.01 mm at 0.41 THz, which is consisted with the simulated results in Fig. 4.

The normalized coupling coefficient κ between the dielectric waveguide and the plasmonic waveguide can be calculated through the overlap integral [19]:

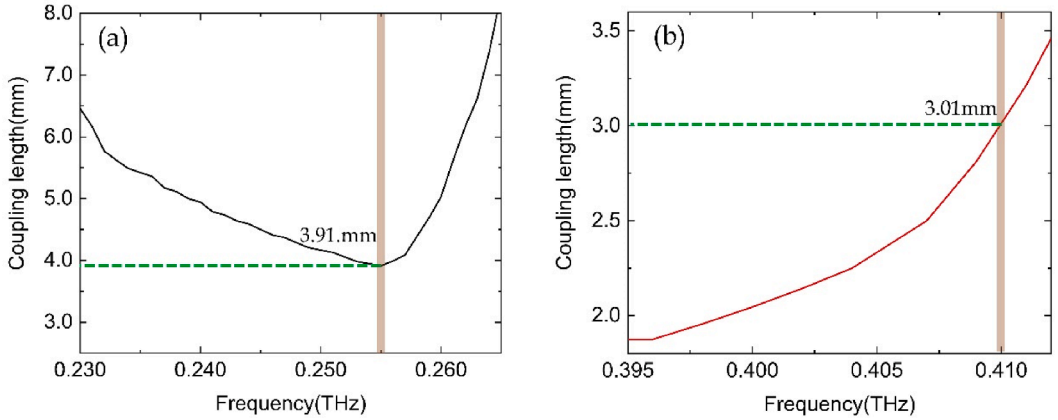

Fig. 5. (a) The coupling length from 0.23 THz to 0.265 THz for the low spoof SPPs mode, which is 3.91 mm at 0.255 THz (b) The coupling length from 0.395 THz to 0.415 THz for the high spoof SPPs mode, which is 3.01 mm at 0.41 THz.

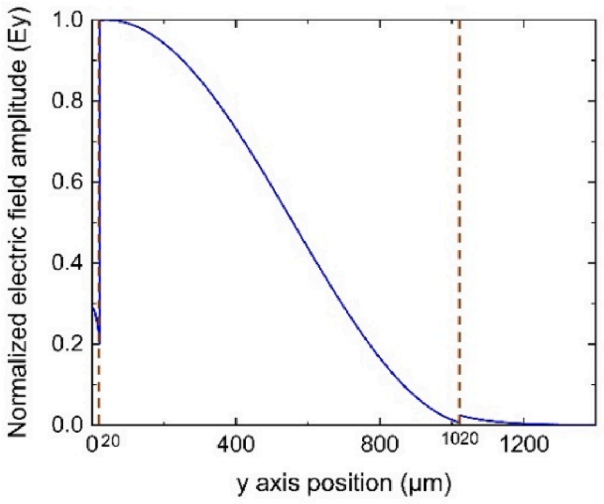

Fig. 6. The normalized field amplitude distribution with $t = 20$ μm at $\lambda_0 = 400$ μm.

$$\kappa = \frac{\left[\int \vec{E}1 \cdot \vec{E}2^{*} ds\right]^2}{\int |E_1|^2 ds \int |E_2|^2 ds} \tag{3}$$

where E_1 and E_2 are the electric field amplitude of dielectric mode and spoof SPPs mode, s is the cross section in the integration.

Fig. 6 plotted the normalized electric field amplitude with respect to the y axis. There is the "hole" power distribution in the alumina layer. Fig. 7(a) shows the effect of the groove depth on coupling efficiency by $t = 20$ μm. We can see that as h increases, the normalized coupling efficiency slightly decreased due to the gradually increased field mismatch between dielectric and spoof SPPs. The results for $h = 150$ μm and 350 μm fit well with the simulated results. Moreover, if the propagation length is fixed, the propagation difference $\Delta k = k_{zd}$-k_{zm} is linear to the phase difference. So we can monitor phase difference in replace of the propagation difference. Fig. 7(b) plotted the normalized coupling efficiency with respect to phase difference $\Delta\varphi$. When the phase difference reaches π, the maximum mode power can be transferred from the dielectric waveguide to the plasmonic waveguide. If the phase difference is 0.5π or 1.5π, THz wave is partly coupled to spoof SPPs, resulting in low coupling efficiency [16] (Fig. 7b).

Experimental details

The experiment is being operated in our work. A THz time-domain spectroscope (FiCO, @Zomega Corp.) was used to test the transmittance of the device, with a valid bandwidth from 0.1 to 1.6 THz [34]. We impulse the THz radiation from one side of the coupling system consisted of plasmonic waveguides with ribbon waveguides and detect the outgoing spectra from the other side. Moreover, the dielectric ribbon waveguides can guide waves at submillimeter wavelength while maintain low dielectric loss [28,30]. The reference signal is obtained by inputting THz pulse from one side of the ribbon waveguide and detecting from the other side. The measured THz time-domain and frequency amplitude spectra after propagating through the proposed structure (black line) and the ribbon waveguide (blue line) are displayed in Fig. 8(a), respectively. The transmission from the ribbon waveguide was used as the reference signal $E_r(\omega)$, and then measurement through the coupling structure was used as the sample signal $E_s(\omega)$. Thus, the coupling efficiency of the coupled system η is as follows:

$$\eta = |E_s(\omega)|/|E_r(\omega)| \tag{4}$$

We substitute the experimental data into Eq. (4) to calculate the coupling efficiency, which is 33% at 0.28 THz and 30% at 0.47 THz. In Fig. 2, the simulated coupling efficiency is around 51% and 63% at

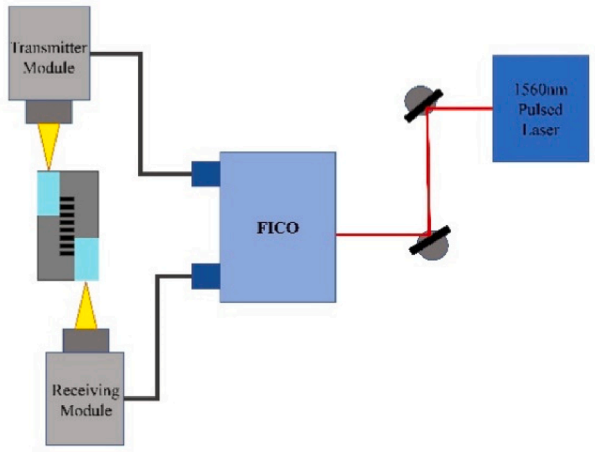

Fig. 7b. The schematic diagram of experimental system, the yellow triangle represents the probe, the rectangle between represents the structure. (For interpretation of the references to colour in this figure legend, the reader is referred to the web version of this article.)

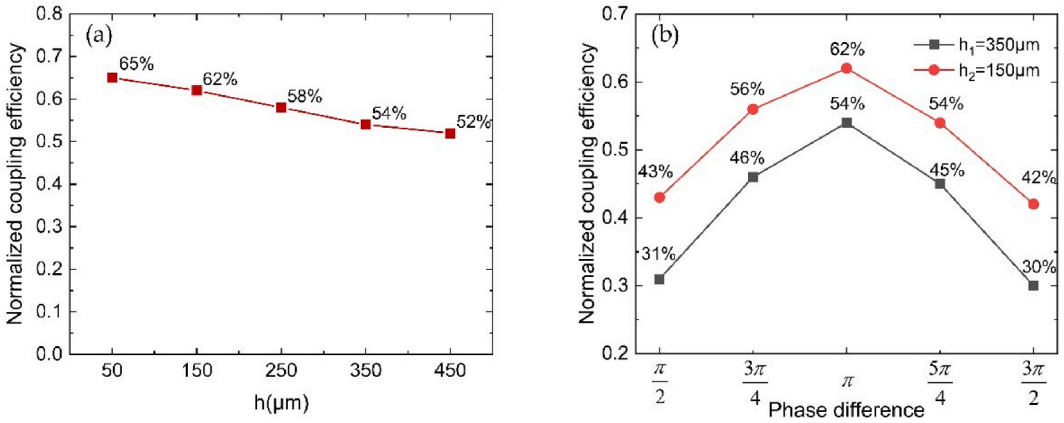

Fig. 7a. (a) The effect of the groove depth on coupling efficiency by $t = 20$ μm. (b) The relationship between phase difference and coupling efficiency, reaches 54% for h_1 and 62% for h_2 when the phase difference is π. the coupling length are set as 3.91 mm (0.255 THz) and 3.01 mm (0.41 THz), then find out the coupling effect under different phase difference.

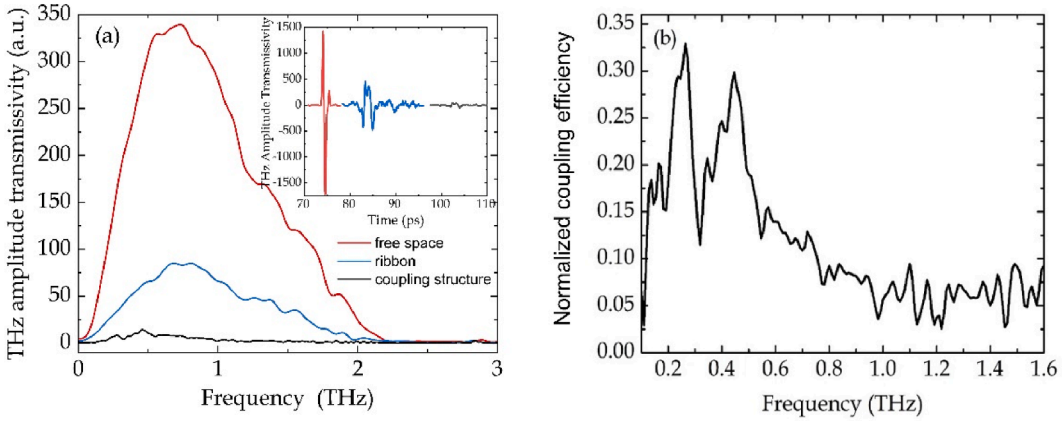

Fig. 8. (a) THz amplitude transmissivity of the measured propagating pulse through free space (red), ribbon waveguide (blue) and coupling structure (black) (Inset: time domain spectra). (b) Normalized coupling structure, which is obtained by divided THz amplitude transmissivity of the coupled structure (black line) to that of ribbon waveguide (blue line). (For interpretation of the references to colour in this figure legend, the reader is referred to the web version of this article.)

0.255 THz and 0.41 THz, respectively. The result of the experiment fit well with the simulated result. The deviation of the resonance frequencies might be due to the inaccurate size of fabricated metal grating. The manufacturing process and the environmental impact also lead to experimental data errors.

Conclusion and prospective

In conclusion, we have designed, fabricated and characterized a coupling structure composed of dual-band plasmonic waveguide and dielectric waveguide. We obtained the coupling length through the simulated dispersion curve. The coupling efficiency at the resonance frequencies have also been investigated. We can observe experimentally that the coupling efficiency reaches 33% at 0.28 THz and 30% at 0.47 THz normalized by that of ribbon waveguide. The proposed method is expected to create new and exciting avenues in the development of coupling and spoof SPPs transmitting device in the THz spectral range. The coupling efficiency of this method still have large space to improve. In further research, we can connect the network analyzer through VDI extenders to realize better excitation effects [35].

CRediT authorship contribution statement

Wenwei Shen: . **Jingya Xie:** Methodology, Formal analysis. **Xiaofei Zang:** Supervision, Validation. **Li Ding:** Writing - review & editing. **Lin Chen:** Conceptualization, Writing - original draft, Writing - review & editing.

Declaration of Competing Interest

The authors declare that they have no known competing financial interests or personal relationships that could have appeared to influence the work reported in this paper.

Acknowledgments

This Project was supported by the National key R&D Program of China (2018YFF01013003), the Program of Shanghai Pujiang Program, China (No. 17PJD028), the National Natural Science Foundation of China (Nos. 61671302, 61988102 and 61722111), the Shuguang Program Supported by Shanghai Education Development Foundation and Shanghai Municipal Education Commission, China (No. 18SG44), the 111 Project (D18014), the International Joint Lab Program supported by Science and Technology Commission Shanghai Municipality (17590750300).

Disclosures

The authors declare no competing financial interests.

Appendix A. Supplementary data

Supplementary data to this article can be found online at https://doi.org/10.1016/j.rinp.2020.103653.

References

[1] Mendis R, Grischkowsky D. Undistorted guided-wave propagation of subpicosecond terahertz pulses. Opt Lett 2001;26(11):846. https://doi.org/10.1364/OL.26.000846.
[2] Chen L, Gao C, Xu J, Zang X, Cai B, Zhu Y. Observation of electromagnetically induced transparency-like transmission in terahertz asymmetric waveguide-cavities systems. Opt Lett 2013;38(9):1379. https://doi.org/10.1364/OL.38.001379.
[3] Chen L, Zhu Y, Zang X, Cai B, Li Z, Xie Le, Zhuang S. Mode splitting transmission effect of surface wave excitation through a metal hole array. Light Sci Appl 2013;2(3):e60. https://doi.org/10.1038/lsa:2013.16.
[4] Maier Stefan A, Steve R, Andrews L Martín-Moreno, García-Vidal FJ. Terahertz surface plasmon-polariton propagation and focusing on periodically corrugated metal wires. Phys Rev Lett 2006;97:176805. https://doi.org/10.1103/physrevlett.97.176805.
[5] Williams CR, Andrews SR, Maier SA, Fernández-Domínguez AI, Martín-Moreno L, García-Vidal FJ. Highly confined guiding of terahertz surface plasmon polaritons on structured metal surfaces. Nature Photon 2008;2(3):175–9. https://doi.org/10.1038/nphoton.2007.301.
[6] Shen L, Chen X, Yang T-J. Terahertz surface plasmon polaritons on periodically corrugated metal surfaces. Opt Express 2008;16(5):3326. https://doi.org/10.1364/OE.16.003326.
[7] Zhu W, Agrawal A, Nahata A. Direct measurement of the Gouy phase shift for surface plasmon-polaritons. Opt Express 2007;15(16):9995–10001. https://doi.org/10.1364/oe.15. 009995.
[8] Zhu W, Agrawal A, Nahata A. Planar plasmonic terahertz guided-wave devices. Opt Express 2008;16:6216–26. https://doi.org/10.1364/cleo.2009.cwg2.
[9] Chen L, Xu N, Singh L, Cui T, Singh R, Zhu Y, Zhang W. Defect-induced fano resonances in corrugated plasmonic metamaterials. Adv Opt Mater 2017;5(8):1600960. https://doi.org/10.1002/adom.201600960.
[10] Chen L, Wei Y, Zang X, Zhu Y, Zhuang S. Excitation of dark multipolar plasmonic resonances at terahertz frequencies. Sci Rep 2016;6:22027. https://doi.org/10.1038/srep22027.
[11] Chen L, Liao D-G, Guo X-G, Zhao J-y, Zhu Y-M, Zhuang S-L. Terahertz time-domain spectroscopy and micro-cavity components for probing samples: a review. Frontiers Inf Technol Electronic Eng 2019;20(5):591–607. https://doi.org/10.1631/FITEE.1800633.
[12] Saxler J, Gómez Rivas J, Janke C, Pellemans HPM, Bolívar PH, Kurz H. Time-domain measurements of surface plasmon polaritons in the terahertz frequency range. Phys. Rev. B 2004;69(15). https://doi.org/10.1103/PhysRevB.69.155427.
[13] Ng B, Wu J, Hanham SM, Fernández-Domínguez AI, Klein N, Liew YF, Breese MBH, Hong M, Maier SA. Spoof plasmon surfaces: a novel platform for THz sensing. Adv Opt Mater 2013;1(8):543–8. https://doi.org/10.1002/adom.201300146.
[14] Chen L, Ge Y, Zang X, Xie J, Ding L, Balakin AV, et al. Tunable phase transition via radiative loss controlling in a terahertz attenuated total reflection based metasurface. IEEE Trans Terahertz Sci Technol 2019;9(6):643–50. https://doi.org/10.1109/tthz. 2019.2937504.

[15] Martl M, Darmo J, Unterrainer K, Gornik E. Excitation of terahertz surface plasmon polaritons on etched groove gratings. J. Opt. Soc. Am. B 2009;26(3):554. https://doi.org/10.1364/JOSAB.26.000554.
[16] Zhang Y, Xu Y, Tian C, Xu Q, Zhang X, Li Y, Zhang X, Han J, Zhang W. Terahertz spoof surface-plasmon-polariton subwavelength waveguide. Photon. Res. 2018;6(1):18. https://doi.org/10.1364/PRJ.6.000018.
[17] Gaborit G, Armand D, Coutaz J-L, Nazarov M, Shkurinov A. Excitation and focusing of terahertz surface plasmons using a grating coupler with elliptically curved grooves. Appl Phys Lett 2009;94(23):231108. https://doi.org/10.1063/1.3153125.
[18] Jeon T-I, Grischkowsky D. THz Zenneck surface wave (THz surface plasmon) propagation on a metal sheet. Appl Phys Lett 2006;88(6):061113. https://doi.org/10.1063/1.2171488.
[19] Gong M, Jeon TI, Grischkowsky D. THz surface wave collapse on coated metal surfaces. Opt Express 2009;17(19):17088–101. https://doi.org/10.1364/oe.17.017088.
[20] He X, Lin F, Liu F, Shi W. Tunable strontium titanate terahertz all-dielectric metamaterials. J Phys D Appl Phys 2020;53(15):155105. https://doi.org/10.1088/1361-6463/ab6ccc.
[21] Peng J, He X, Shi C, Leng J, Lin F, Liu F, Zhang H, Shi W. Investigation of graphene supported terahertz elliptical metamaterials. Physica E 2020;124:114309. https://doi.org/10.1016/j.physe.2020.114309.
[22] He X, Lin F, Liu F, Zhang H. Investigation of phonon scattering on the tunable mechanisms of terahertz graphene metamaterials. Nanomaterials 2019;10(1):39. https://doi.org/10.3390/nano10010039.
[23] Xia S, Zhai X, Wang L, Lin Q, Wen S. Excitation of crest and trough surface plasmon modes in in-plane bended graphene nanoribbons. Opt Express 2016;24(1):427–36. https://doi.org/10.1364/oe.24.007436.
[24] Xia S-X, Zhai X, Wang L-L, Sun B, Liu J-Q, Wen S-C. Dynamically tunable plasmonically induced transparency in sinusoidally curved and planar graphene layers. Opt Express 2016;24(16):17886. https://doi.org/10.1364/OE.24.017886.
[25] Gao Z, Wu L, Gao F, Luo Y, Zhang B. Spoof plasmonics: from metamaterial concept to topological description. Adv Mater 2018:1706683. https://doi.org/10.1002/adma.201706683.
[26] Zhang X, Xu Q, Xia L, Li Y, Gu J, Tian Z, Ouyang C, Han J, Zhang W. Terahertz surface plasmonic waves: a review. Adv Photonics 2020;2(1):014001. https://doi.org/10.1117/1.ap.2.1.014001.
[27] Ferguson B, Zhang X-C. Materials for terahertz science and technology. Nat Mater 2002;1(1):26–33. https://doi.org/10.1038/nmat708.
[28] Yeh C, Shimabukuro F, Siegel PH. Low-loss terahertz ribbon waveguides. Appl Opt 2005;44(28):5937. https://doi.org/10.1364/AO.44.005937.
[29] Yeh C, Shimabukuro FI, editors. The Essence of Dielectric Waveguides. Boston, MA: Springer US; 2008. https://doi.org/10.1007/978-0-387-49799-0_11. 339–355p.
[30] Mendis R, Grischkowsky D. Plastic ribbon THz waveguides. J Appl Phys 2000;88(7):4449. https://doi.org/10.1063/1.1310179.
[31] See Supplemental Material for a detailed description of optimum thickness of the alumina and the polypropylene and corresponding Supplemental Figures.
[32] Chen L, Cao Z, Ou F, Li H, Shen Q, Qiao H. Observation of large positive and negative lateral shifts of are reflected beam from symmetrical metal-cladding waveguides. Opt Lett 2007;32:1432–4. https://doi.org/10.1364/ol.32.001432.
[33] Gao X, Shi JH, Ma HF, Jiang WX, Cui TJ. Dual-band spoof surface plasmon polaritons based on composite-periodic gratings. J Phys D Appl Phys 2012;45(50):505104. https://doi.org/10.1088/0022-3727/45/50/505104.
[34] Wang X, Li Y, Cai B, Zhu YiMing. High refractive index composite for broadband antireflection in terahertz frequency range. Appl Phys Lett 2015;106(23):231107. https://doi.org/10.1063/1.4922574.
[35] Xie J, Zhu X, Zang X, Cheng Q, Chen L, Zhu Y. Terahertz integrated device: high-Q silicon dielectric resonators. Opt Mater Express 2018;8(1):50–8. https://doi.org/10.1364/ome.8.000050.